Soft Matter

Dynamic Article Links

Cite this: *Soft Matter*, 2012, **8**, 4635

www.rsc.org/softmatter

PAPER

Frictional forces in polyelectrolyte brushes: effects of sliding velocity, solvent quality and salt

Florent Goujon,[a] Aziz Ghoufi,[b] Patrice Malfreyt*[a] and Dominic J. Tildesley[c]

Received 22nd December 2011, Accepted 14th February 2012
DOI: 10.1039/c2sm07450h

We report dissipative particle dynamics (DPD) simulations of grafted polymer brushes under shear at three separation distances. We investigate the impact of the shear on single monolayers and compressed bilayers formed by neutral and charged polymer chains. The dependence of the friction on the solvent quality is studied for different charge fractions in two compressed polymer brushes. The change in the frictional forces upon the addition of the salt is analyzed in terms of change in the interpenetration coefficient. We complete this study by a description of the brush structure including ordering, composition, tilt and local electroneutrality at different separation distances, salt concentrations, charge fractions and shear rates. Interestingly, some heterogeneities in the monomer density profiles of polyelectrolyte brushes appear under shear and vanish upon addition of salt.

1 Introduction

The lubrication properties of neutral polymer brushes, formed by grafting neutral polymer chains to a flat surface, have been investigated extensively by experiment.[1–7] The low frictional forces can be explained by the ability to support large normal forces due to the limited interpenetration between opposing grafted surfaces. However, the weak resistance to shear can depend on the quality of the solvent, the compression and the surface coverage.[8,9]

More recently, a further substantial reduction in the friction has been observed for polyelectrolyte brushes (densely grafted of charged polymers).[10–14] This reduction of friction was ascribed to the decrease of the interpenetration between the two opposing charged brushes and the presence of hydration layers around charged groups in the sheared interpenetration zone.[11,15] However, the underlying physical mechanism remains poorly understood.

A number of theories[16–26] have been developed to study the physical behavior of these polyelectrolyte brushes but very few studies[23] have been devoted to the friction in sliding polyelectrolyte brushes. Computer simulation methods are an efficient tool to investigate the physics of two interacting polyelectrolyte brushes under shear provided that we can reach the required length and timescales to study most polymer phenomena. One way to overcome these limitations is to use a coarse-grained description. Indeed, in recent simulations of polyelectrolyte brushes,[20,21,27–30] the polymer chains were modelled using a bead–spring approach. The coarse graining of this model is then limited by the use of the Lennard-Jones potential that requires a relatively small timestep to integrate the equations of motion. Additionally, in these simulations, the solvent was not treated explicitly.

An alternative approach is the dissipative particle dynamics (DPD) method proposed by Hoogerbrugge and Koelman.[31,32] DPD is a stochastic dynamics method in which the individual particles (beads) represent a packet of atomistic degrees of freedom (*i.e.* region of the solvent or the polymer). As a consequence of this coarse-graining, the conservative interactions are soft. The dissipative and Brownian forces are short-ranged and pairwise additive so that the dynamics obeys Newton's third law. Thus, the DPD method satisfies the Navier–Stokes equation. The first advantage of DPD is that it can use time steps up to an order of magnitude larger than those typically used in MD simulations. Secondly, and unlike Brownian dynamics (BD), hydrodynamic interactions are properly accounted for. Thirdly, it is straightforward to model the solvent particles explicitly. Recent progress in DPD simulations allow us to modify the standard DPD algorithm by the addition of forces preventing bond crossing between polymers[33–35] and electrostatic interactions to model polyelectrolytes.[36–39]

In the past, we have successfully applied the dissipative particle dynamics (DPD) method to study the equilibrium properties[33,40,41] and rheological properties[8,9,35] of neutral polymer brushes. However, the modelling of charged polymer chains has required the calculation of long range electrostatic interactions at a mesoscopic level. We have tested two approaches on a model of electrolyte and polyelectrolyte brushes.[38] The first method, developed by Groot,[36] is based upon the particle–particle particle–mesh (PPPM) method with a charge distribution

[a]*Clermont Université, Université Blaise Pascal, Laboratoire de Thermodynamique et Interactions Moléculaires, CNRS, UMR 6272, LTIM, BP 10448, F-63000 CLERMONT-FERRAND. E-mail: Patrice.Malfreyt@univ-bpclermont.fr; Fax: +33 473 40 53 28; Tel: +33 473407204*
[b]*Institut Physique de Rennes, CNRS, UMR 6251, IPR, 263 Avenue Général Leclerc, F-35042 Rennes*
[c]*Unilever Research, Port-Sunlight, Bebington, Wirral CH63 3JW, UK*

function adapted to the use of a soft potential. The second approach, developed by Gonzáles-Melchor,[37] used the Ewald[42] technique with a charge distribution on the DPD particles. The structural and mechanical properties of a single polyelectrolyte brush were found to be essentially equivalent for the PPPM and Ewald methods. The main conclusions we can draw from our mesoscale simulations of single and interacting polyelectrolyte brushes are as follows: i) the dependence of the brush height on the grafting density and of the charge fraction is typical of the nonlinear osmotic brush regime,[20,21,29] ii) all the counterions are confined inside the brush in line with the small values of the Gouy–Chapman length,[38,39,43] iii) the interpenetration coefficient between two interacting polyelectrolyte brushes follows the scaling law of the nonlinear osmotic brush regime,[43,44] iv) the polyelectrolyte brushes at equilibrium can support a larger load with respect to that calculated in neutral brushes at the same overlap. DPD simulations were also carried out to investigate the dependence of the interpenetration coefficient on the grafting density, polymer size and separation distance.[45]

Our longer-term objective is to understand the mechanisms involved in the reduction of friction in polyelectrolyte brushes with respect to neutral brushes by examining the role played by the electrostatic interactions in the frictional behavior. However, the comparison of the friction between charged and neutral polymer brushes requires modeling two interacting polymer brushes at different separation distances where the solvent between the two surfaces is in equilibrium with a reservoir of the bulk fluid at the same temperature and chemical potential. Additionally, the friction between charged and neutral polymer brushes must be represented as a function of a compression ratio D/D_o[13] where D_o is the separation distance for which the properties of the two brushes are equivalent to those of single brush. The values of D_o are strongly dependent on the charge fraction and will be determined in this work. Before investigating the compression of polyelectrolyte brushes under shear deformation, here we propose to investigate the impact of the shear on the properties of charged polymer brushes at three fixed separation distances and fixed total number density. We aim to address the following fundamental questions:

- How does the friction change with the sliding velocity at different separation distances?
- How does the solvent quality change the frictional forces of compressed neutral and charged polymer brushes?
- What is the dependence of the friction on the salt concentration?
- How does the shear impact on the internal structure of polymer brushes?

In the next section, we present the conventional, spring-repulsion and electrostatic forces used in the DPD model. The results are discussed in section 3. Finally, we conclude in section 4 providing a brief summary of our main results.

2 The dissipative particle dynamics (DPD) model

2.1 Standard DPD forces

In the DPD approach, solvent particles are coarse grained into soft beads that interact with the pairwise additive force $\mathbf{f}_i$ defined as the sum of three contributions

$$\mathbf{f}_i = \sum_{j \neq i} (\mathbf{f}_{ij}^{C} + \mathbf{f}_{ij}^{R} + \mathbf{f}_{ij}^{D}) \quad (1)$$

where $\mathbf{f}_{ij}^{C}$, $\mathbf{f}_{ij}^{R}$ and $\mathbf{f}_{ij}^{D}$ are the conservative, random and dissipative forces, respectively. The conservative repulsive force $\mathbf{f}_{ij}^{C}$ derives from a soft interaction potential and is expressed as

$$\mathbf{f}_{ij}^{C} = \begin{cases} a_{ij}\omega_C\left(r_{ij}\right)\hat{\mathbf{r}}_{ij} & \left(r_{ij} < r_c\right) \\ 0 & \left(r_{ij} \geq r_c\right) \end{cases} \quad (2)$$

where a_{ij} is the maximum repulsion parameter between particles i and j, r_{ij} is the relative displacement of particles i and j and $\hat{\mathbf{r}}_{ij}$ is the corresponding unit vector. r_c is the cutoff radius. The weight function $\omega_c(r_{ij})$ is equal to $1 - r_{ij}/r_c$ for $r_{ij} \leq r_c$ and vanishes for $r_{ij} \geq r_c$. The dissipative and random forces are given by

$$\mathbf{f}_{ij}^{D} = -\dot{\gamma}\omega^{D}(r_{ij})(\hat{\mathbf{r}}_{ij}\cdot\mathbf{v}_{ij})\hat{\mathbf{r}}_{ij} \quad (3)$$

$$\mathbf{f}_{ij}^{R} = \sigma\omega^{R}\left(r_{ij}\right)\theta_{ij}\frac{1}{\sqrt{\delta\, t}}\,\hat{\mathbf{r}}_{ij} \quad (4)$$

where δt is the time step, $\mathbf{v}_{ij} = \mathbf{v}_i - \mathbf{v}_j$ is the relative velocity, σ is the amplitude of the noise, and θ_{ij} is a random Gaussian number with zero mean and unit variance. γ and σ are the dissipation strength and noise strength, respectively. The terms $\omega^{D}(r_{ij})$ and $\omega^{R}(r_{ij})$ are dimensionless weighting functions. Español and Warren[46] have shown that the system will sample the canonical ensemble and obey the fluctuation–dissipation theorem if the following conditions are satisfied.

$$\gamma = \frac{\sigma^2}{2k_B T} \quad \text{and} \quad \omega^{D}\left(r_{ij}\right) = \left(\omega^{R}\left(r_{ij}\right)\right)^2 \quad (5)$$

where k_B is Boltzmann's constant and T is the temperature. The weighting function $\omega^{R}(r_{ij})$ is chosen to be equal to $\omega^{C}(r_{ij})$.

When modelling polymers, the integrity of the chain is ensured by an additional spring force between neighboring beads given by

$$\mathbf{f}_{ij}^{S} = -k_s\left(r_{ij} - r_0\right)\hat{\mathbf{r}}_{ij} \quad (6)$$

where the equilibrium bond distance r_0 is 0.85 and the spring constant $k_s = 200$. This pairwise force[36] is then added to the sum of the DPD conservative force of eqn (1).

2.2 Bond crossings

The forces used in the standard DPD model cannot prevent the bond crossings because of the soft repulsion between the beads. This leads to many violations of the topology of the polymer chains and ignores entanglements. We have included an additional repulsion force between the chain segments to prevent such crossings on the basis of the Kumar and Larson spring–spring repulsion model.[47] The entanglement force, $\mathbf{f}_{ij}^{E}$, is

$$\mathbf{f}_{ij}^{E} = \begin{cases} a_{ij}^{E}\left(1 - \dfrac{d_{ij}}{r_c^{E}}\right)\hat{\mathbf{d}}_{ij} & \left(d_{ij} < r_c^{E}\right) \\ 0 & \left(d_{ij} \geq r_c^{E}\right) \end{cases} \quad (7)$$

where $\hat{\mathbf{d}}_{ij} = \mathbf{d}_{ij}/d_{ij}$ is the corresponding unit vector and d_{ij} is the minimum distance between the two interacting bond segments i and j. a_{ij}^{E} is the maximum repulsion value and r_c^{E} represents the cutoff value for the entanglement interactions. The force is applied to the polymer beads by using a simple lever rule: each bead receives a fraction of the force corresponding to its distance

from the segment interaction point.[47] The calculation of $\mathbf{f}_{ij}^{E}$, the tests for topology violation and a detailed study of the efficiency of such a model in DPD and polymer brushes can be found in a previous paper.[33]

2.3 Ewald summation (EW3DC) method

The method recently proposed by González-Melchor *et al.*[37] consists in combining the Ewald technique[42] and a charge distribution for the particles. In the case of an electroneutral system formed by N particles, every one carrying a point charge q_i at position r_i in a volume $V = L_x L_y L_z$, the long range electrostatic interactions are decomposed into contributions in the real space and in the reciprocal space

$$U\left(\mathbf{r}^N\right) = \frac{1}{4\pi\varepsilon_0\varepsilon_r}\left[\sum_i \sum_{j>i} q_i\, q_j \frac{\operatorname{erfc}\left(\alpha r_{ij}\right)}{r_{ij}} + \frac{2\pi}{V}\sum_{k\neq 0}^{\infty} Q\left(h\right) S\left(\mathbf{h}\right) S\left(-\mathbf{h}\right) - \frac{\alpha}{\sqrt{\pi}}\sum_i^N q_i^2\right] \quad (8)$$

where $\operatorname{erfc}(x)$ is the complementary error function. α is chosen so that only pair interactions in the central cell need to be considered in evaluating the first term of eqn (8). The functions $Q(h)$ and $S(\mathbf{h})$ are defined using eqn (9) and 10

$$Q(h) = \exp(-h^2/4\alpha^2)/h^2 \quad (9)$$

$$S\left(\mathbf{h}\right) = \sum_{i=1}^{N} q_i \exp(i\,\mathbf{h}\cdot\mathbf{r}_i) \quad (10)$$

where the components of the reciprocal vector $\mathbf{h}$ are defined as $2\pi(l/L_x, m/L_y, n/L_z)$ where l,m,n take values $0,\pm1,\pm2,\ldots,\pm\infty$.

To remove the divergence of the Coulombic potential at $r = 0$, Alejandre and coworkers[37] have considered a Slater-type charge distribution centred on DPD particles of the form

$$f\left(r\right) = \frac{q}{\pi\lambda^3}\exp(-2r/\lambda) \quad (11)$$

where λ is the decay length of the charge. The distribution is normalised to q.

The magnitude of the reduced force between two charge distributions is then given by the sum of a pairwise additive contribution $\mathbf{f}_{ij}^{E,R}$ coming from the real space and a non-pairwise additive contribution $\mathbf{f}_i^{E,K}$ from the reciprocal space term. These two contributions are given by the following expressions

$$\mathbf{f}_{ij}^{E,R} = \frac{4\pi}{\Gamma}\, q_i\, q_j \left[\frac{2\,\alpha r_{ij}}{\sqrt{\pi}}\exp\left(-\alpha^2\, r_{ij}^2\right) + \operatorname{erfc}\left(\alpha\, r_{ij}\right)\right]\times \left[1-\exp\left(-2\,\beta r_{ij}\right)\left(1+2\,\beta\, r_{ij}\left(1+\beta r_{ij}\right)\right)\right]\frac{\mathbf{r_{ij}}}{r_{ij}^3} \quad (12)$$

$$\mathbf{f}_i^{E,K} = -\frac{4\,\pi}{\Gamma} q_i \left[\frac{2\,\pi}{V}\sum_{\mathbf{h}\neq 0} Q(h)\mathbf{h}\times \operatorname{Im}\left[\exp(-i\mathbf{h}.\mathbf{r_i})S(\mathbf{h})\right]\right] \quad (13)$$

where Im denotes the imaginary part of the complex variable.

2.4 Total DPD force

To remove the net dipole moment of the simulation cell, a z-component force is added for each bead

$$\mathbf{f}_{i,z} = -\frac{\Gamma}{V}\, M_z \quad (14)$$

where M_z is the z-component of the net dipole moment of the simulation cell given by $\sum_i q_i\, \mathbf{r_i}$ and V the volume expressed in reduced units. This contribution is the correction term from Yeh and Berkowitz[48] which results from the plane-wise summation method proposed by Smith.[49] Finally, the total force acting on the ith particle becomes

$$\mathbf{f}_i = \mathbf{f}_i^{E,K} + \mathbf{f}_{i,z} + \sum_{j\neq i}^{N}\left(\mathbf{f}_{ij}^{C} + \mathbf{f}_{ij}^{R} + \mathbf{f}_{ij}^{D} + \mathbf{f}_{ij}^{E,R}\right) + \sum_{k\neq i}^{N_c}\left(\mathbf{f}_{ik}^{S}\right) + \sum_{l\neq i}^{N_i}\left(\mathbf{f}_{il}^{E}\right) \quad (15)$$

where N is to the total number of beads in the system, N_c is the number of connected polymer beads to i and N_i the number of interacting bonds on i. The pairwise $\mathbf{f}_{ij}^{E,R}$ force is then added to sum of the conservative, dissipative and random pairwise forces whereas $\mathbf{f}_i^{E,K}$ and $\mathbf{f}_{i,z}$, which are not pairwise additive, are added to the force $\mathbf{f}_i$ acting on the particle i.

2.5 Rheological properties

The components of the pressure tensor used for the determination of the friction coefficient are calculated along the z-axis using the Irving–Kirkwood[50,51] definition. The profiles of the pressure are calculated by splitting the cell into slabs of width Δz. The $p_{\alpha\beta}$ component is composed of a kinetic contribution $p_{\alpha\beta}^{kin}(z)$ and a virial part $p_{\alpha\beta}^{conf}(z)$ defined as

$$p_{\alpha\beta}^{kin}\left(z\right) = \frac{1}{V}\left\langle \sum_{i,\alpha,\beta} H\left(z_i\right) m_i\left[\left(v_i\right)_\alpha - \left(u\right)_\alpha\right]\left[\left(v_i\right)_\beta - \left(u\right)_\beta\right]\right\rangle \quad (16)$$

$$p_{\alpha\beta}^{conf}\left(z\right) = \frac{1}{A}\left\langle \sum_{i=1}^{N-1}\sum_{j>i}^{N}\left(r_{ij}\right)_\alpha\left(\mathrm{f}_{ij}\right)_\beta \frac{1}{\left|z_{ij}\right|}\,\theta\left(\frac{z-z_i}{z_{ij}}\right)\,\theta\left(\frac{z_j-z}{z_{ij}}\right)\right\rangle \quad (17)$$

where $\langle\ldots\rangle$ denotes the configurational average and α and β represent x, y and z directions, m_i and $(v_i)_\alpha$ are the mass and velocity of particle i, respectively. $V = L_x L_y \Delta z$ is the volume of the basic slab, $H(z_i)$ is a top-hat function and $(u)_\alpha$ is the α component of the streaming velocity. Whereas $(u)_x$ is a measure of the induced flow field, $(u)_y$ and $(u)_z$ are essentially zero for all z. f_{ij} represents the sum of the pairwise additive forces in eqn (15) and θ is a unit step function. When the force is not pairwise additive such as $\mathbf{f}_i^{E,K}$, we used the Harasima definition for the pressure calculation.[50,52]

The friction coefficient defined in eqn (18) is averaged over the slabs along the z-direction as the ratio of the off-diagonal pressure tensor component in the shear direction to the normal component $p_{zz}(z)$

$$\langle\varepsilon\rangle = \langle\varepsilon(z)\rangle_z = -\left\langle\frac{p_{xz}\left(z\right)}{p_{zz}\left(z\right)}\right\rangle_z \quad (18)$$

The shear viscosity is calculated in the middle of the simulation cell from the profile of $\eta(z)$ as

$$\eta(z) = -\frac{\langle p_{xz}(z)\rangle}{\left\langle \frac{\mathrm{d}u_x(z)}{\mathrm{d}z}\right\rangle} \quad (19)$$

A previous[8] study shows from the viscosity profiles that the minimum of the viscosity is observed in the middle of the pore in the region of the highest solvent density.

2.6 DPD Parameters

In the simulation, the particle mass, temperature, interaction range are chosen as units of mass, energy and length, hence $m = k_BT = r_c = 1.0$. The unit of time τ becomes then $r_c\sqrt{m/k_B\,T}$. The coupling constant Γ is given by $e^2/(k_BT\varepsilon_0\varepsilon_r r_c)$ where e is the electronic charge, $\varepsilon_0 = 8.85418782 \times 10^{-12}$ C^2 J^{-1} m^{-1} is the permeability of free space, $\varepsilon_r = 78.3$ the relative permittivity of water at 298 K. Using these values, we calculate $r_c = 6.46$ Å and $\Gamma = 13.87$. As already discussed by Groot and Rabone,[53] the time scale is fixed by matching the diffusion constant of water. For a repulsion parameter $a = 25$, we find that the natural unit of time τ is 160 ps. The Bjerrum length, defined by $\lambda_B = e^2/(4\pi k_BT\varepsilon_0\varepsilon_r)$, characterizes the length scale at which two units charges interact with thermal energy K_BT in a medium of dielectric constant ε. With the parameters used in this work, λ_B is equal to 1.11 in reduced DPD units.

2.7 Simulation details

The system of grafted bilayers consists of two planar solid surfaces, each composed of two layers of 572 DPD particles. The two surfaces are positioned at the top and the bottom of the simulation cell along the z direction at a separation distance D. The two surfaces are coated with $N_p = 96$ polymer chains which are randomly grafted by an harmonic force acting between the ends particles of the chains and the particles of the first layer of the wall. Each chain contains $N_b = 20$ polymer beads which are negatively charged. The surface coverage defined by $\rho_a = N_p/(L_xL_y)$ is 0.5 in reduced units. The percentage of wall particles of the last layer connected to the first beads of the polymer chains is then 1/6. Different charge fractions of the polymer chains f are studied: 1.0 (completely negatively charged); 0.5 (half charged); and zero (neutral). To preserve the neutrality, there are $N_+ = f \times N_p \times N_b$ counterions which are positively charged. The number of solvent particles is adjusted to yield a total number density of 4.0 between the two surfaces. The cell dimensions are $L_x = 16.07r_c$, $L_y = 11.77r_c$. L_z is the dimension of the primary cell. To respect the supercell approximation, the simulation cell is elongated along the z direction by placing an empty space of at least twice the space of the region occupied by fluid. The periodic boundary conditions are then applied in the three directions. Typical views of the simulation cell are given in Fig. 1.

The a_{ij} parameters are set to 25.0 for all interactions in the case of athermal conditions. It means that the polymer–polymer, polymer–solvent, solvent–solvent, solvent–counterion and polymer–counterion energy contributions use the same a_{ij} parameter. The values $a_{ij}^{ent} = 20$ and $r_c^E = 0.40$ were found to be optimal[33,35] to prevent bond crossings with the DPD parameters used in our simulations. We found that $\sigma/(\delta t)^{1/2} = 100$ is satisfactory to obtain a very good agreement between the calculated and target temperature in the non-equilibrium simulations under shear. The equations of motions are integrated using a modified version of the velocity–Verlet algorithm.[36] The force is updated once per iteration and because the force depends on the velocities, the velocity in the next time step has to be estimated by a predictor algorithm. The velocity is then corrected in the last step. The reduced time-step δt was taken to 0.01 for all the simulations reported in the paper. The simulation consisted of an equilibration period of 100 000 steps followed by an acquisition period of 500 000 steps. The DPD simulations were performed over 12 processors at a time and take between 8 h and 2 days each, depending on the system size.

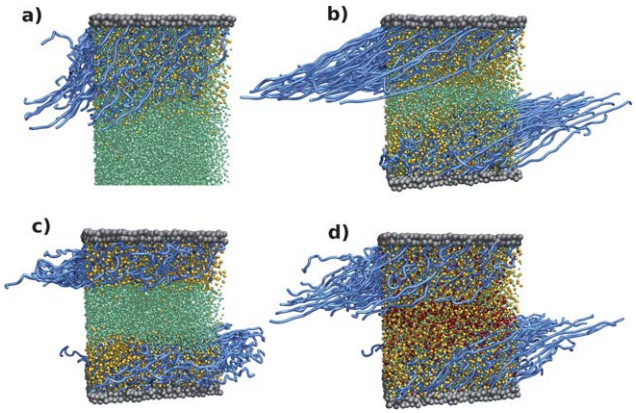

Fig. 1 Typical configurations of sheared polyelectrolyte brushes for fully charged polymer chains. a) A single monolayer corresponding to an infinite separation distance. Parts b) c) and d) show two interacting polyelectrolyte brushes at a compression ratio $D/D_o = 0.5$ with b) under athermal solvent conditions; c) poor solvent conditions and d) athermal conditions with the addition of salt ($c_s = 0.500$). The wall particles are represented by gray particles, the polymer beads are blue, the solvent is green, the counterions (positively charged) are yellow and the salt particles (negatively charged) are red.

The shear rate is applied to the system by imposing a movement on the surface particles along x-axis. The amount δx is added to the reference lattice:

$$\delta x = \pm\frac{\dot{\gamma}_a D}{2}\,\delta t \quad (20)$$

where $\dot{\gamma}_a$ is the applied shear rate expressed in units of $(k_BT/mr_c^2)^{1/2}$. The sign depends on which surface (top or bottom) is considered, as they slide along opposite directions.

3 Results and discussions

3.1 Effect of sliding velocity on friction

We report the dependence of the friction on the sliding velocity at three different separation distances. We study a grafted monolayer (see Fig. 1a) corresponding to a bilayer at infinite separation and two bilayers at weak and strong compression ratios D/D_o. D_o corresponds to the minimum separation distance of a grafted bilayer in which the shape of the monomer density profile and the brush height are strictly identical to those calculated in a single brush. The values of D_o are 24.0, 32.0 and 36.0 and those of the brush height (h) are 7.2, 9.5 and 11.4 for neutral, half and fully charged polymer chains, respectively. The values of

D_o and h calculated from the first moment[39,43] show that $D_o/2h_o \approx 1.6$ is required to obtain two unperturbed brushes. The weak compression regime investigated in this paper corresponds to $D/D_o = 0.8$ with values of D ranging from 19.2 to 28.8 as the charge fraction increases from 0 to 1. The strong compression regime is modeled here by a ratio D/D_o of 0.5 with D increasing from 12 ($f = 0$) to 18 ($f = 1$). The shear rate $\dot{\gamma}_a$ is varied from 0.0 to 0.25 in steps of 0.025.

Fig. 2a shows the dependence of the friction coefficient of polymer brushes on the shear rate for different separation distances and charge fractions. For the single brush at an infinite separation distance, we observe a linear dependence of the friction on the sliding velocity for the neutral, half fully charged and fully charged brushes. At the weak compression ($D/D_o = 0.8$), the friction starts to show a nonlinear behavior at the smallest velocities. This effect is much more marked at the largest compression where the nonlinear viscoelastic behavior of the polymer brushes is exhibited over a large range of shear rates. Since the simulations are carried out at fixed total number density and due to the lubricant properties of the solvent particles,[9] it is not possible to make a direct comparison of the friction between charged and neutral brushes from our constant-NVT simulations.

Fig. 2b shows the viscosity of the solvent in the middle of the pore as a function of the shear rate. In weakly compressed polymer brushes, the viscosity remains constant with respect to the shear rate. This underlines the Newtonian behavior of the solvent. We also observe in Fig. 2b the shear-thinning behavior of the polymer brushes at strong compressions where the reduction of the viscosity with increasing shear rate reaches 55% and 48% for neutral and fully charged polymer chains, respectively. Fig. 2c shows the dependence of the interpenetration coefficient[54] on the sliding velocity. In all cases, we observe a decrease of the overlap between the two brushes as a function

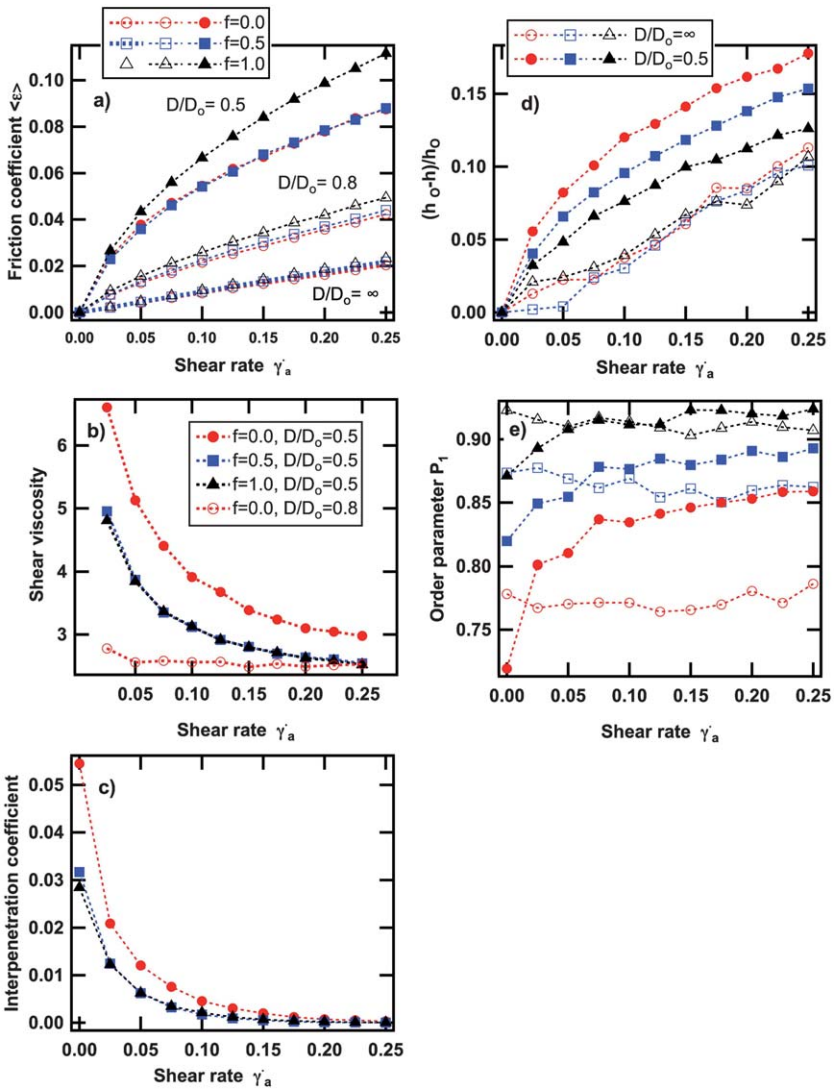

Fig. 2 a) The friction coefficient, b) the shear viscosity and c) the interpenetration coefficient as a function of the shear rate for different compression ratios, d) relative brush shrinkage and e) order parameter as a function of the sliding velocity for a single monolayer ($D/D_o = \infty$) and a compressed bilayer ($D/D_o = 0.5$).

of the shear rate. This decrease is much more marked in the case of neutral brushes that exhibit a stronger overlap and an higher viscosity than those of charged brushes.

To investigate the deformation of the brushes under flow, we plot in Fig. 2d the relative brush shrinkage $\delta h = (h_o - h)/h_o$ for a single monolayer and a strongly compressed bilayer as a function of the charge fraction. h_o is defined here as the brush height at zero shear rate. In the case of a monolayer, the relative deformation of the brush δh is the same for the neutral and charged polymer brushes. For a strong compression ratio in the bilayer, we observe that the deformation under shear decreases with increasing charge fraction. This means that the polyelectrolyte brushes are less susceptible to deformation in solvent flows than neutral brushes. This is in line with the behavior predicted by theory.[55] The brushes of fully charged chains are completely stretched in monolayers with an elongation of about 70% of their contour length. This extension decreases to 55% in the bilayer at the strongest compression.

The internal ordering of the layer as a function of shear rate is presented in Fig. 2e for the monolayer and the compressed bilayer at $D/D_o = 0.5$ for $f = 0$,0.5 and 1.0. The internal ordering against the director can be estimated from the order parameter P_1 as

$$P_1 = \frac{1}{N}\left\langle \sum_i \mathbf{e}_i \cdot \mathbf{d} \right\rangle \tag{21}$$

where $\mathbf{d}$ is the director and corresponds to the average orientation of the layer. It is the eigenvector corresponding to the largest eigenvalue of the $\mathbf{Q}$ tensor defined as $\mathbf{Q} = \frac{1}{N}\left(\sum_i \mathbf{e}_i\,\mathbf{e}_i - \frac{1}{3}\,I\right)$ where the sum is over all polymer chains. $P_1 = 1$ means that all the grafted chains perfectly align with the director of the layer. As the polymer brush system is sheared, the polymer chains tend to tilt in the direction of the imposed shear. The tilt is more pronounced at high shear rate and for neutral brushes. For neutral brushes at $\dot{\gamma}_a = 0.25$, the average tilt of the monolayer is about 58° whereas it is 75° for a compressed bilayer. The tilt also increases with the compression ratio: the tilt of the fully charged polymer layer is 33° and 63° for the monolayer and compressed bilayers, respectively. It is very interesting to observe in Fig. 2d that the order parameter is independent of the shear rate in monolayers. We also check that the internal order parameter of monolayers increases with the charge fraction. In bilayer structures, the shear impacts significantly on the internal ordering in the range of sliding velocities smaller than 0.1. However, the magnitude of the change in P_1 due to the shear decreases with increasing charge fraction suggests that the shear further affects the neutral brushes in terms of internal ordering. By contrast, the extent of ordering is largest within the layer of polyelectrolyte brushes. It might be explained by the presence of counterions that significantly order the layer. Indeed, the degree of condensation[39,43] is almost 100% for both the monolayer and bilayer structures indicating that all the counterions are trapped into the brush layers within the range of shear rate used here. By increasing the internal ordering of the charged brushes, the strength of the interaction between the polymer bead and the counterion makes the polyelectrolyte brushes less susceptible to any modifications of the internal alignment of the layer by shear flow. A typical snapshot of a polyelectrolyte under shear in athermal solvent conditions is shown in Fig. 1b.

3.2 Friction-dependence on solvent quality

The quality of the solvent is changed through the polymer–solvent interaction. We define the quality of the solvent as

$$\Delta a_{\text{pol-sol}} = a_{\text{pol-sol}} - \frac{1}{2}\left(a_{\text{sol-sol}} + a_{\text{pol-pol}}\right) \tag{22}$$

If the repulsive parameter $a_{\text{pol-sol}}$ is set higher than those for all the other interactions, $\Delta a_{\text{pol-sol}}$ is positive and the polyelectrolyte is in a poor solvent condition. In contrast, a lower value of $a_{\text{pol-sol}}$ gives a negative $\Delta a_{\text{pol-sol}}$ contribution and the polymers are in a good solvent condition. $\Delta a_{\text{pol-sol}}$ was varied from −15 to +15. This is the range of solvent qualities explored in this paper.

Fig. 3a shows the effect of the solvent quality on the friction coefficient in a strongly compressed bilayer ($D/D_o = 0.5$) at three charge fractions for a shear rate of 0.1. For neutral brushes, the friction is very small and does not change in the range of poor solvent quality ($\Delta a_{\text{pol-sol}} > 0$). The friction coefficient starts to

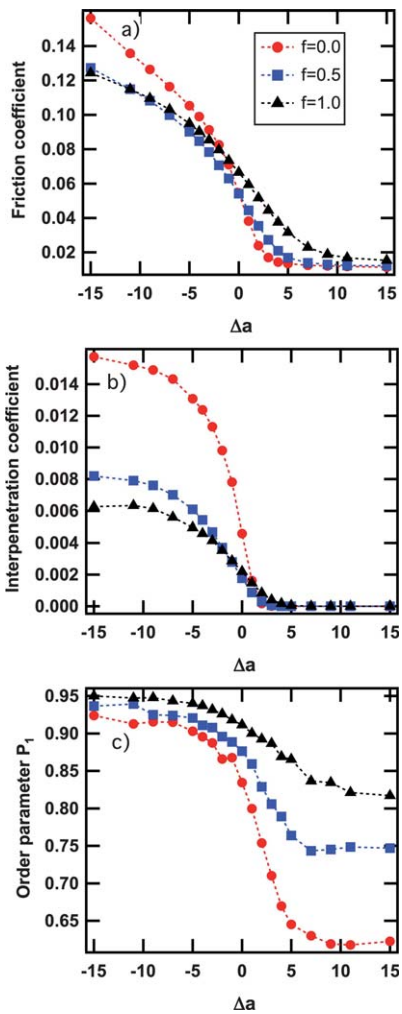

Fig. 3 The dependence of the friction a), interpenetration b) and order parameter c) on the solvent quality defined by Δa.

rise steeply from $\Delta a = 5$ and keeps increasing as the solvent quality improves. In the case of polyelectrolyte brushes, the range of poor solvent quality for which the friction remains unchanged is reduced and the friction starts to increase progressively from poor solvent conditions. Fig. 1c shows a typical configuration of sheared polyelectrolyte brushes in poor solvent conditions. The presence of electrostatic interactions in the fully charged polymer chains increases the friction in poor solvent conditions and decreases the frictional forces in good solvent conditions. This means that the change in the friction due to the solvent quality is attenuated in polyelectrolyte brushes. Additionally, a plateau appears in the region of good solvents for polyelectrolyte brushes whereas the friction of neutral brushes continue increasing in this region. Additionally, we observe that in good solvent conditions the friction in polyelectrolyte brushes becomes smaller than is the case for neutral brushes. However, we must perform non-equilibrium simulations at fixed solvent chemical potential to definitively conclude on the lubricant properties of polyelectrolyte brushes.

Fig. 3b shows the dependence of the interpenetration coefficient[8,9,41] on the solvent quality. Interestingly, we observe significant changes between charged and neutral brushes in good solvent conditions. We find that the overlap between the two opposing layers is greater for neutral brushes than for charged brushes due to the electrostatic repulsive interactions between the end groups of the polymer chains. We also show a direct correlation between the friction coefficient and the interpenetration even though the changes in the interpenetration between charged and neutral brushes are not proportionally reproduced in the frictional forces.

Fig. 3c shows the evolution of the order parameter as a function of the solvent quality. First, $\Delta a = 5$ is the threshold from which P_1 starts to rise. Second, we observe that the internal ordering of the layer increases with the charge fraction in bad solvent conditions, whereas it is almost independent of the charge fraction in good solvents. This means that the change in the internal alignment of the layer with respect to the solvent quality is much less important in polyelectrolyte brushes. Improving the solvent quality in neutral brushes can improve the degree of ordering of the layer by 50%. This property is strongly impacted by the charge fraction in bad solvents. In terms of internal ordering of the layer, we show that the solvent quality has much less effect on fully charged polymer brushes compared to neutral polymer brushes. The P_1 parameter of polyelectrolyte brushes in poor solvent conditions corresponds to a value of an internal alignment of neutral brushes in athermal solvent conditions. The average tilt of the layer in polyelectrolyte brushes does not depend on the solvent quality for this compression ratio: we only observe a variation of 3° over the entire range of solvent qualities.

3.3 Impact of salt concentration on friction

In this section, we investigate the effect of adding salt on the frictional forces of fully charged polymer brushes in athermal solvent conditions at a compression ratio $D/D_o = 0.5$ and a shear rate of 0.1. A typical configuration of polyelectrolyte brushes with salt is given in Fig. 1d. When no salt is added, the system is formed by 3840 polymer beads, 3840 counterions and 5942 solvent particles. A salt concentration $c_s = 0.010$ corresponds to the addition of 34 mobile positive ions and 34 mobile negative ions in the total volume. The number of solvent particles is then adjusted to keep a total density number of 4.0. The salt concentration was varied from 0.0 to 0.5. The conservative interactions for the solvent–salt, polymer–salt and salt–salt are identical to those for all the other interactions ($a_{ij} = 25$).

Fig. 4 shows the dependence of the friction coefficient on the salt concentration. We add for completeness the change in the interpenetration coefficient with respect to the salt concentration. Over the salt concentration range investigated here, the friction coefficient has decreased by 1.5 and the interpenetration by 10 with respect to the salt-free athermal solvent conditions. In contrast, the properties such as P_1 order parameter, average tilt of the layer and viscosity remain almost unchanged upon the addition of salt. Interestingly, the brush height decreases only 6% over the range of salt concentrations used here. A clear correlation between the frictional forces and the overlap between the opposing brushes is established in the presence of salt in two compressed polyelectrolyte brushes. The friction and interpenetration coefficient of the polyelectrolyte brushes for $c_s = 0.5$ are equivalent to those of the brushes in a poor solvent defined by $\Delta a = +3$.

3.4 Effect of shear on brush structure

In this section, we discuss the density profiles of polymer beads, counterions and coions along the normal to the surfaces in order to examine the effects of shear on the brush structure. Fig. 5a shows the monomer density profiles of the monolayer brush for neutral and fully charged chains at $\dot{\gamma}_a = 0$ and 0.1. The brush height is about 7.2 for a neutral monolayer and 11.4 for a fully charged polyelectrolyte corresponding to a stretching of about 44% and 75% from their contour length, respectively. The density profiles clearly show that the charged polymer chains extend further in the direction normal to the surface and that the shear flow has little influence on the profiles. We only observe a slight reduction in the width of the brush in line with the differences observed in the profiles of the region of the tails. The shape of the monomer density profiles remain parabolic for all the charge fractions and the shear rates.

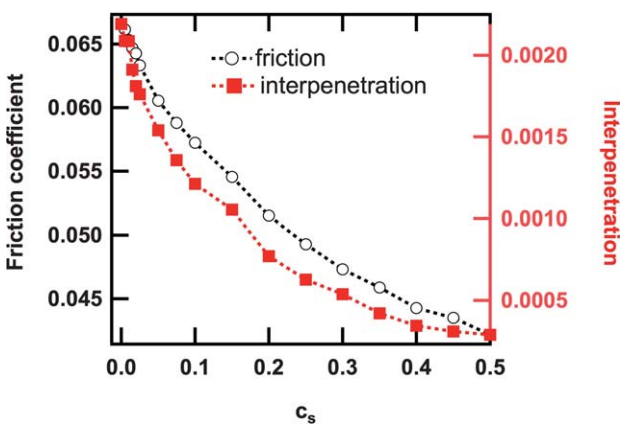

Fig. 4 The friction coefficient and interpenetration as a function of the salt concentration c_s in the case of a bilayer at $D/D_o = 0.5$ and $\dot{\gamma}_a = 0.1$.

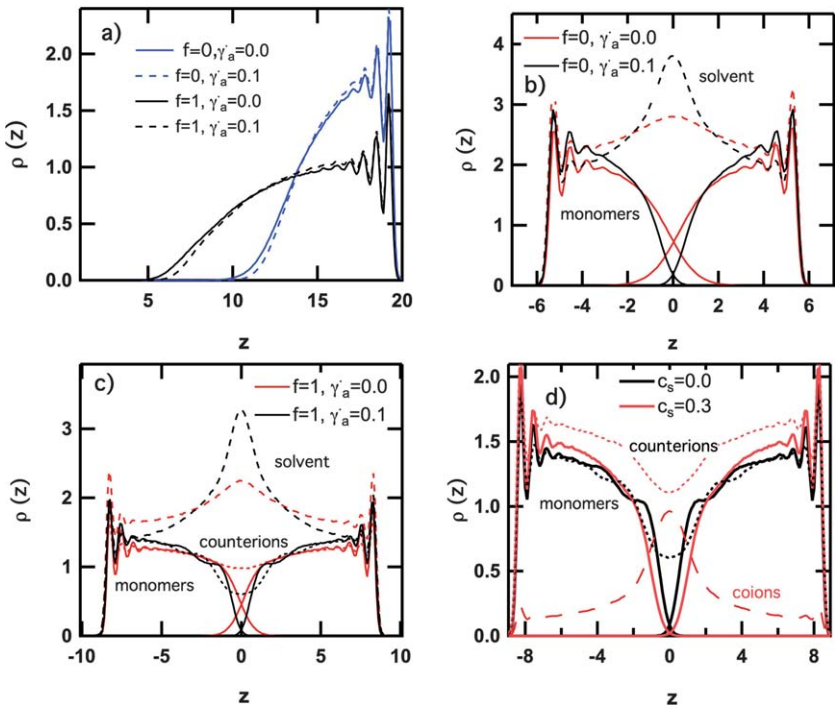

Fig. 5 a) The monomer density profiles of neutral and charged monolayers at equilibrium and under shear, b) the monomer and solvent density profiles of bilayers formed by neutral chains for $\dot{\gamma}_a = 0.0$ and 0.1, c) monomer, counterions and solvent density profiles of polyelectrolytes at $D/D_o = 0.5$, d) the monomer, counterions and coions density profiles at two salt concentrations.

Fig. 5b show that the density profiles of the neutral compressed polymer brushes are more sensitive to the shear than those of monolayers. The average tilt of the layer in the flow direction increases from 39° to 71° as the shear rate is varied from 0 to 0.1. This is in line with a reduction of the width of the brush accompanied by a smaller overlap between the two opposing layers. When no shear rate is applied under athermal solvent conditions, Fig. 5b shows that the solvent density profiles is almost uniform in the direction normal to the surface. This indicates that a large fraction of solvent particles penetrate in the polymer chains. Upon shear flow, there is an increase in the solvent density in the interpenetration zone facilitated by the retraction of the tails in the opposing brushes.

In the case of compressed polyelectrolyte brushes, the monomer density profiles of Fig. 5c become more step-like in comparison to the parabolic shape of neutral brushes. Interestingly, Fig. 5c shows that the shear acts to retract the charged brushes, to shift the solvent in the overlap region and also to create some discontinuities in the shape of the monomer profile. These inhomogeneities in $\rho(z)$ will be discussed later through the analysis of the charge distributions. We also observe that the profile of the counterions matches well with that of the monomer in the polymer regions, indicating that the counterions are almost all contained in the brush layers in agreement with a degree of condensation close to 100%. We also observe a decrease in the number of counterions accompanied by a decrease of solvent particles in the overlap region of sheared polyelectrolyte brushes with respect to the sheared neutral brushes.

Fig. 5d shows that the heterogeneities of the grafted layers vanish upon the addition of salt. We also find that the profiles of the compressed brushes under shear change from a rather step-like shape to a parabolic form with increasing salt concentration. The profiles show a retraction of the tails of the brushes with a brush height decreasing from 8.3 to 7.6 upon addition of salt. The coion density profiles of Fig. 5d for $c_s = 0.3$ show that they are significantly distributed in the polymer-free region even if a small fraction of these coions can enter the brush layers. The density of the counterions in the salted brush regime for $c_s = 0.3$ becomes larger than that of the polymer beads to maintain a local neutrality due to the presence of coions. The presence of all these species in the brush region leads to the salt screening of the electrostatic interactions. As a consequence, the structural brush properties such as brush height and shape tend to those of the neutral brush as salt is added.

In Fig. 6 we show the profiles of the sum of the charged species (coions, polyions and counterions) as a function of z for fully charged polymer chains under shear in the cases of free-salt and salt with athermal solvent conditions. We add for comparison the charge profiles of polyelectrolyte brushes with no shear applied. All the profiles show that the electroneutrality is satisfied at each z in the polymer rich region even if some oscillations appear close to the surfaces due to the layering of the grafted polymers. At equilibrium, the polyelectrolyte brushes show a slight enhancement in the counterion particles at the middle of the box leading to the formation of a charge layer in the overlap zone. When shear is applied, we observe a significant increase of the charge layer at the middle of the box with the formation of two smaller dipoles on each side. The formation of these two dipoles is due to the presence of heterogeneities in $\rho(z)$ induced by the shear flow: the profiles of the counterions and polymer beads shown in Fig. 5d are no

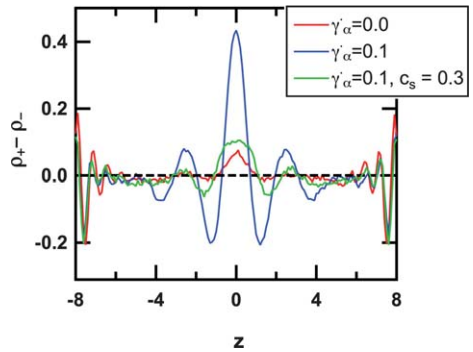

Fig. 6 The local charge net as a function of the distance from the grafting surface at equilibrium, under shear and with salt.

longer superimposed in this zone of heterogeneities. One way to cancel these heterogeneities and the induced charge layers is to add salt. Indeed, Fig. 6 shows that adding salt promotes the recovery of a charge profile very close to that of polyelectrolyte brushes at equilibrium.

We have analyzed the formation of the heterogeneities inside the brushes induced by the shear deformation. To this end, we represent the distributions of the mean squared length λ_1 of the longest axis of the polymer chains calculated from diagonalizing the squared radius of gyration tensor $\mathbf{R}_g^2$. The diagonalization of $\mathbf{R}_g^2$ results in three eigenvalues λ which sum to the mean squared radius of gyration $\langle R_g^2 \rangle$, and the largest of which corresponds to an eigenvalue vector representing the long axis of the polymer chain. In the case of single layers, we observe broad distributions for λ_1 covering a range from 0 to 20 for both equilibrium and sheared brushes. For a compressed neutral bilayer at equilibrium, the distribution is much narrower and the range of possible values for λ_1 is reduced by half. For polyelectrolyte brushes at equilibrium, we observe only one peak with a broader distribution with respect to neutral brushes. When shear is applied, the λ distributions are dramatically modified. The first peak is significantly reduced in magnitude and the distribution becomes almost homogeneous and extends over a large range. For charged brushes under shear, the magnitude of the first peak is further reduced and a second peak appears at large values of λ with an homogeneous distribution of chain lengths between these two peaks. This means that the shear flow broadens the distribution of polymer lengths and induces in the case of charged polymer chains two distinct folded and unfolded conformations for the polymer chain. The next question is if the folded and unfolded chain conformations interact with the same number of counterions. To this end, we define a new parameter called X_i defined as the number of unique counterions for which a polymer chain i is the nearest neighbor. This parameter is then normalized by the number of beads in the chain. As a consequence, the average value of X over all the chains is 1 due to the total charge neutrality in the box. Thus, the case of $X_i = 1$ means that each polymer bead of the chain interacts with a unique counterion. If $X_i < 1$, the number of unique counterions available in the close neighborhood of the chain i is smaller that the number of beads, leading to a deficit of counterions. If $X_i > 1$, the chain i interacts preferentially with more unique counterions than is required for local electroneutrality. Fig. 7b shows a correlation between X_i and λ_1 for single monolayers and compressed bilayers of fully charged chains at equilibrium and under shear. In the cases of monolayers, the number of unique counterions in close association with the polymer chain is less than 1.0 except for $\lambda_1 = 10$. This means that the different conformations of the polymer chains in the 0–20 λ_1 range are arranged to maintain local neutrality with a small fraction of counterions at the rim of the brush. For charged bilayers at equilibrium, the situation is different: values of $\lambda_1 > 5$ require values of $X_i > 1$ whereas for $\lambda_1 < 5$, we observe a deficit of close counterions. Under shear, the chains are further stretched with respect to neutral sheared brushes and chains with large values of λ_1 induce relatively large values of X_i compared to equilibrium brushes. The only way of satisfying the neutrality in the brush is that some chains compensate the effects of the longest chains by folding with smaller values of λ_1 and X_i leading to a redistribution of the counterions within the layer. This explains the heterogeneities in $\rho(z)$ of polyelectrolyte brushes that are observed under shear and not detected at equilibrium. These discontinuities in $\rho(z)$ are mainly due to a broad distribution of chain conformations and their interaction with counterions. When adding salt to the brushes, the total number of available counterions is increased. As a consequence, the heterogeneities in $\rho(z)$ disappear for a salt concentration of $c_s = 0.3$ (see Fig. 5d).

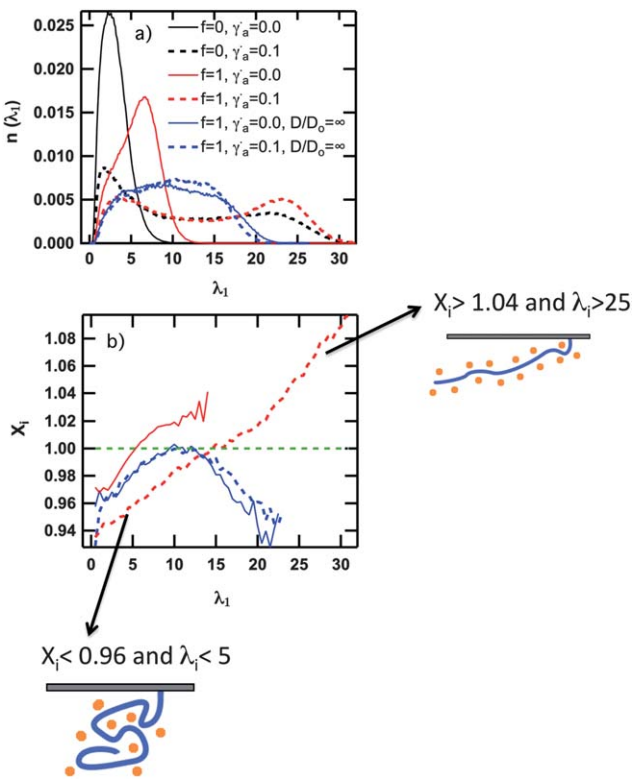

Fig. 7 a) The distributions of λ_1 for different separation distances and charge fractions b) the X_i parameter as a function of λ_1 with the same legend as that used in a). The green dotted line $X_i = 1$ is a guide for the eye. The inset illustrates two typical conformations of folded and unfolded polymer chains with the corresponding counterions.

4 Conclusions

We have performed non-equilibrium dissipative particle dynamics simulations of neutral and charged polymer brushes under shear to investigate the effects of the sliding velocities, the solvent quality and the salt concentration on the frictional forces and internal structure of the brushes for three different separation distances.

The friction coefficient of single layers shows a linear dependence on the sliding velocity independent of the charge fraction. The shear-thinning behavior of compressed bilayer brushes has been established over a large range of shear rates. We have also demonstrated that the polyelectrolyte brushes are less susceptible to deformation under shear than neutral brushes. However, the internal ordering in the polyelectrolyte brushes is greater than that in neutral brushes.

The effect of the solvent quality has been studied in two strongly compressed polymer brushes formed by neutral and charged chains. A clear correlation between the friction coefficient and the amount of overlap between the two brushes has been established in charged and neutral systems. The interpenetration coefficient of polyelectrolyte brushes was found to be reduced in comparison to that of neutral brushes. The solvent quality does not significantly impact the internal ordering in polyelectrolyte brushes whereas it can increase the degree of ordering by 50% in neutral brushes.

The dependence of the friction on salt concentration also shows a correlation between the friction and the interpenetration in compressed polyelectrolyte brushes under athermal solvent conditions. A salt concentration of $c_s = 0.5$ has the same impact on the frictional forces as a poor solvent quality defined by $\Delta a = +3$.

We have completed this study by the analysis of the density profiles of the monomers, counterions and solvent along the normal to the surface. The monomer density profiles are step-like in charged brushes and parabolic in neutral ones for a relatively strong compression ratio. Heterogeneities have been established in the monomer and counterions density profiles of compressed polyelectrolyte brushes under shear, whereas the same profiles do not exhibit any discontinuities in brushes at equilibrium and upon addition of salt. These discontinuities in $\rho(z)$ have been explained in terms of the broad distributions of chain conformations and the number of available counterions around the chains.

We plan to extend this work by the study of the dependence of the frictional forces on the surface separation distance in neutral and charged polymer brushes under shear at fixed solvent chemical potential. We aim at investigating the lubricant properties of the polyelectrolyte brushes in terms of the viscosity, friction and composition of the interpenetration region between the two opposing layers.

Acknowledgements

This work was granted access to the HPC resources of IDRIS under the allocation 2011-i2011092119 made by GENCI (Grand Equipement National de Calcul Intensif).

References

1 J. Klein, *Pure Appl. Chem.*, 1992, **64**, 1577.
2 J. Klein, E. Kumacheva, D. Mahalu, D. Perahia and L. J. Fetters, *Nature*, 1994, **370**, 634.
3 J. Klein, *Annu. Rev. Mater. Sci.*, 1996, **26**, 581.
4 P. A. Schorr, T. C. B. Kwan, S. M. K. II, E. S. G. Shaqfey and M. Tirrell, *Macromolecules*, 2003, **36**, 389.
5 R. Tadmor, J. Janik and J. Klein, *Phys. Rev. Lett.*, 2003, **91**, 115503.
6 M. T. Muller, X. Yan, S. Lee, S. S. Perry and N. D. Spencer, *Macromolecules*, 2005, **38**, 3861.
7 M. T. Muller, X. Yan, S. Lee, S. S. Perry and N. D. Spencer, *Macromolecules*, 2005, **38**, 5706.
8 D. Irfachsyad, D. J. Tildesley and P. Malfreyt, *Phys. Chem. Chem. Phys.*, 2002, **4**, 3008.
9 F. Goujon, P. Malfreyt and D. J. Tildesley, *Mol. Phys.*, 2005, **103**, 2675.
10 J. U. Kim and M. W. Matsen, *Macromolecules*, 2009, **42**, 3430.
11 U. Raviv, S. Giasson, N. Kampf, J. F. Gohy, R. Jerome and J. Klein, *Nature*, 2003, **425**, 163.
12 U. Raviv, S. Giasson, N. Kampf, J. F. Gohy, R. Jerome and K. Klein, *Langmuir*, 2008, **24**, 8678.
13 B. Liberelle and S. Giasson, *Langmuir*, 2008, **24**, 1550.
14 I. E. Dunlop, W. H. Briscoe, S. Titmuss, R. M. J. Jacobs, V. L. Osborne, S. Edmondson, W. T. S. Huck and J. Klein, *J. Phys. Chem. B*, 2009, **113**, 3947.
15 U. Raviv and J. Klein, *Science*, 2002, **297**, 1540.
16 S. Misra, S. Varanasi and P. P. Varanasi, *Macromolecules*, 1989, **22**, 4173.
17 P. Pincus, *Macromolecules*, 1991, **24**, 2912.
18 O. V. Borisov, E. B. Zhulina and T. M. Birshtein, *Macromolecules*, 1994, **27**, 4795.
19 S. Misra, M. Tirrell and W. Mattice, *Macromolecules*, 1996, **29**, 6056.
20 A. Naji, R. R. Netz and C. Seidel, *Eur. Phys. J. E*, 2003, **12**, 223.
21 H. Ahrens, S. Förster, C. A. Helm, N. A. Kumar, A. Naji, R. R. Netz and C. Seidel, *J. Phys. Chem. B*, 2004, **108**, 16870.
22 P. M. Biesheuvel, W. M. de Vos and V. M. Amoskov, *Macromolecules*, 2008, **41**, 6254.
23 J. B. Sokoloff, *J. Chem. Phys.*, 2008, **129**, 014901.
24 J. U. Kim and M. W. Matsen, *Macromolecules*, 2009, **42**, 3430.
25 S. He, H. Merlitz, L. Chen, J. Sommer and C. Wu, *Macromolecules*, 2010, **43**, 7845.
26 M. W. Matsen, *Eur. Phys. J. E*, 2011, **34**, 45.
27 F. S. Csajka and C. Seidel, *Macromolecules*, 2000, **33**, 2728.
28 C. Seidel, *Macromolecules*, 2003, **36**, 2536.
29 N. A. Kumar and C. Seidel, *Macromolecules*, 2005, **38**, 9341.
30 O. J. Hehmeyer and M. J. Stevens, *J. Chem. Phys.*, 2005, **122**, 134909.
31 P. J. Hoogerbrugge and J. M. V. A. Koelman, *Europhys. Lett.*, 1992, **19**, 155.
32 J. M. V. A. Koelman and P. J. Hoogerbrugge, *Europhys. Lett.*, 1993, **21**, 363.
33 F. Goujon, P. Malfreyt and D. J. Tildesley, *J. Chem. Phys.*, 2008, **129**, 034902.
34 F. Lahmar, C. Tzoumanekas, D. N. Theodorou and B. Rousseau, *Macromolecules*, 2009, **42**, 7485.
35 F. Goujon, P. Malfreyt and D. J. Tildesley, *Macromolecules*, 2009, **42**, 4310.
36 R. D. Groot, *J. Chem. Phys.*, 2003, **118**, 11265.
37 M. González-Melchor, E. Mayoral, M. E. Velazquez and J. Alejandre, *J. Chem. Phys.*, 2006, **125**, 224107.
38 C. Ibergay, P. Malfreyt and D. J. Tildesley, *J. Chem. Theory Comput.*, 2009, **5**, 3245.
39 C. Ibergay, P. Malfreyt and D. J. Tildesley, *J. Phys. Chem. B*, 2010, **114**, 7274.
40 P. Malfreyt and D. J. Tildesley, *Langmuir*, 2000, **16**, 4732.
41 F. Goujon, P. Malfreyt and D. J. Tildesley, *ChemPhysChem*, 2004, **5**, 457.
42 P. P. Ewald, *Ann. Phys.*, 1921, **369**, 253.
43 C. Ibergay, P. Malfreyt and D. J. Tildesley, *Soft Matter*, 2011, **7**, 4900.
44 N. A. Kumar and C. Seidel, *Phys. Rev. E: Stat., Nonlinear, Soft Matter Phys.*, 2007, **76**, 020801.
45 M. Sirchabesan and S. Giasson, *Langmuir*, 2007, **23**, 9713.
46 P. Español and P. B. Warren, *Europhys. Lett.*, 1995, **30**, 191.
47 S. Kumar and R. G. Larson, *J. Chem. Phys.*, 2001, **114**, 6937.
48 I. C. Yeh and M. L. Berkowitz, *J. Chem. Phys.*, 1999, **111**, 3155.
49 E. R. Smith, *Proc. R. Soc. London, Ser. A*, 1981, **375**, 475.
50 J. P. R. B. Walton, D. J. Tildesley, J. S. Rowlinson and J. R. Henderson, *Mol. Phys.*, 1983, **48**, 1357.
51 J. P. R. B. Walton, D. J. Tildesley and J. S. Rowlinson, *Mol. Phys.*, 1986, **58**, 1013.
52 A. Harasima, *Adv. Chem. Phys.*, 1958, **1**, 203.
53 R. D. Groot and K. L. Rabone, *Biophys. J.*, 2001, **81**, 725.
54 F. Goujon, P. Malfreyt and D. J. Tildesley, *Soft Matter*, 2010, **6**, 3472.
55 J. L. Harden, O. V. Borisov and M. E. Cates, *Macromolecules*, 1997, **30**, 1179.

